Transcription elongation rate affects nascent histone pre-mRNA folding and 3′ end processing

Tassa Saldi, Nova Fong, and David L. Bentley

Department of Biochemistry and Molecular Genetics, University of Colorado School of Medicine, Aurora, Colorado 80045, USA

Transcription elongation rate influences cotranscriptional pre-mRNA maturation, but how such kinetic coupling works is poorly understood. The formation of nonadenylated histone mRNA 3′ ends requires recognition of an RNA structure by stem–loop-binding protein (SLBP). We report that slow transcription by mutant RNA polymerase II (Pol II) caused accumulation of polyadenylated histone mRNAs that extend past the stem–loop processing site. UV irradiation, which decelerates Pol II elongation, also induced long poly(A)$^+$ histone transcripts. Inhibition of 3′ processing by slow Pol II correlates with failure to recruit SLBP to histone genes. Chemical probing of nascent RNA structure showed that the stem–loop fails to fold in transcripts made by slow Pol II, thereby explaining the absence of SLBP and failure to process 3′ ends. These results show that regulation of transcription speed can modulate pre-mRNA processing by changing nascent RNA structure and suggest a mechanism by which alternative processing could be controlled.

[*Keywords*: transcription elongation rate; cotranscriptional RNA folding; histone mRNA 3′ end processing; stem–loop binding protein; kinetic coupling]

Supplemental material is available for this article.

Received December 15, 2017; revised version accepted January 23, 2018.

As a gene is transcribed by RNA polymerase II (Pol II), pre-mRNAs undergo multiple processing steps to produce mature mRNAs, including capping, splicing, and 3′ end formation. Because pre-mRNA processing occurs cotranscriptionally, these events can be affected by changes in RNA Pol II modification and kinetics. Differential phosphorylation of the C-terminal domain (CTD) as Pol II travels along a gene allows for spatial coupling of transcription with processing via regulated recruitment of factors that contact this domain. The polar nature of transcription means that it can impose an "order of events" on pre-mRNA processing. For example, selection of an upstream 3′ splice site or poly(A) site can preclude the use of a downstream site, and the choice between alternative processing sites is influenced by the rate of transcription elongation. Elongation rate affects numerous alternative splicing (de la Mata et al. 2003; Ip et al. 2011; Fong et al. 2014) and polyadenylation (Pinto et al. 2011; Liu et al. 2017) decisions. One way that such kinetic coupling operates is by modulating the duration of the "window of opportunity" for processing at upstream sites on the transcript before competing downstream sites are made. This type of kinetic control can regulate alternative splicing within the range of physiological elongation rates that vary between 0.5 kb/min and 5 kb/min (Danko et al. 2013; Fong et al. 2014; Fuchs et al. 2014).

Another way that elongation rate could potentially affect cotranscriptional RNA processing is by altering how the nascent transcript folds (Eperon et al. 1988; Pan and Sosnick 2006; Lai et al. 2013). RNA secondary structure is a critical determinant of splicing (Eperon et al. 1988; Buratti and Baralle 2004), RNA editing (Eggington et al. 2011), alternative polyadenylation (Wu and Bartel 2017), and 3′ processing of replication-dependent (RD) histone mRNAs (Wang et al. 1996). Elongation rate can alter the structure that a nascent transcript adopts by modulating the window of opportunity for upstream sequences to base-pair with alternative downstream complementary elements (Wong and Polisky 1985; Pan and Sosnick 2006). In this way, RNA polymerase speed impacts the formation of transient RNA structures, which unpair and reform multiple times as a transcript assumes its mature structure. Inappropriate cotranscriptional folding can result in kinetic trapping of nonfunctional dead-end RNA structures (Repsilber et al. 1999; Koduvayur and Woodson 2004). There are several well-documented examples in

Corresponding author: david.bentley@ucdenver.edu
Article published online ahead of print. Article and publication date are online at http://www.genesdev.org/cgi/doi/10.1101/gad.310896.117.

Escherichia coli where transcriptional kinetics control in vivo RNA folding (Lewicki et al. 1993; Chao et al. 1995; Pan et al. 1999; Repsilber et al. 1999; Koduvayur and Woodson 2004; Wickiser et al. 2005), but kinetic control of a physiologically relevant RNA structure has yet to be demonstrated in a eukaryote.

Perhaps the best-understood structural element in eukaryotic pre-mRNA processing is the conserved stem–loop (SL) at the 3′ end of RD histone transcripts (Birchmeier et al. 1982). This element is recognized by SL-binding protein (SLBP) (Wang et al. 1996), which stabilizes interaction of U7 snRNP with the histone downstream element (HDE) of the pre-mRNA (Schaufele et al. 1986; Mowry and Steitz 1987; Dominski et al. 1999; Skrajna et al. 2017). Together, SLBP and U7 snRNP direct RNA cleavage 5 bases downstream from the SL. SLBP forms part of a large 3′ end processing complex that includes factors shared with the poly(A) site cleavage machinery, such as the CPSF73 endonuclease and symplekin (Dominski et al. 2005; Kolev and Steitz 2005; Yang et al. 2012). SLBP, CPSF73, symplekin, and CstF77 localize at histone genes by chromatin immunoprecipitation (ChIP), consistent with cotranscriptional 3′ end formation (Glover-Cutter et al. 2008; Sullivan et al. 2009; Hsin et al. 2011). SLBP also interacts with the negative elongation factor (NELF) through Cap-binding complex (CBC), and NELF knockdown impairs histone mRNA 3′ end formation (Narita et al. 2007). Because the SL provides a binding site for SLBP, correct folding of this structure is absolutely essential for normal 3′ processing of histone mRNAs. Substitutions that perturb base-pairing of the stem or alter the identity of unpaired bases 5′ of the stem inhibit SLBP binding and 3′ end processing (Williams et al. 1994; Battle and Doudna 2001; Dominski et al. 2003). When histone mRNA 3′ end processing is disrupted by knockdown of SLBP, NELF, CBC, or CDK9 transcription continues past the normal termination site, and a 3′ end is formed at a distal poly(A) site (Lanzotti et al. 2002; Narita et al. 2007; Pirngruber et al. 2009). Importantly, in terminally differentiated cells, a subset of RD histone genes somehow bypasses the normal 3′ end formation site and switches to produce these long polyadenylated mRNAs (Lyons et al. 2016).

In this report, we examined the effect of transcription elongation rate on histone gene expression. Slow elongation inhibited histone mRNA 3′ end formation, resulting in increased readthrough transcription. Readthrough transcripts accumulated as 3′ extended poly(A)$^+$ histone transcripts. Defective 3′ end processing was associated with a failure of SLBP to localize at histone genes. In an effort to discover a possible reason for this failure, we probed Pol II nascent RNA structure, which revealed that slow elongation prevented formation of the RNA secondary structure required for SLBP binding. These data provide evidence that elongation rate can profoundly affect nascent RNA folding, which can then affect protein binding needed for cotranscriptional RNA processing. These observations raise the interesting possibility that control of elongation rate could be a mechanism used for modulation of alternative RNA processing events in eukaryotes.

Results

Slow transcription causes accumulation of 3′ extended poly(A)$^+$ histone transcripts

We looked for differential expression of total poly(A)$^+$ transcripts in replicate paired-end RNA sequencing (RNA-seq) data sets from HEK293 cell lines that inducibly express α-amanitin-resistant Pol II large subunits that are either a wild-type control, wild-type Am^r, or a slow mutant (R749H) (Fong et al. 2014). The R749H mutation in the funnel domain results in an average elongation rate of 0.5 kb/min, whereas the wild-type α-amanitin-resistant mutant elongates at an average speed of 1.7 kb/min, in good agreement with endogenous Pol II (Fong et al. 2014). We found 1099 up-regulated (>2×; false discovery rate [FDR] < 0.05) and 1480 down-regulated poly(A)$^+$ transcripts in the slow mutant treated with 2.5 µg/mL α-amanitin for 45 h relative to cells expressing the wild-type Am^r Pol II (Supplemental Table S1). Strikingly, among poly(A)$^+$ transcripts, of the 23 RD histone transcripts expressed in our data set, every one was increased in the R749H slow mutant, and 19 out of 23 showed statistically significant increases (FDR < 0.05) (Fig. 1A, black bars). Examination of individual RD histone genes revealed poly (A)$^+$ mRNA-seq reads that extend well past the normal mRNA 3′ end in the slow mutant (Fig. 1B, red arrows). This effect was specific to RD histone genes, as we saw no consistent change in the transcript abundance or length at replication-independent histone genes (Fig. 1B bottom right panel; Supplemental Fig. S1A,B). We confirmed the increase in 3′ extended reads in R749H for a subset of histone genes by quantitative RT–PCR (qRT–PCR) of nuclear poly(A)$^+$ RNA (Fig. 1C). The presence of reads past the 3′ end of RD histone genes in R749H suggested that slow transcription was resulting in 3′ end formation at distal poly(A) sites. To confirm this, we performed 3′ RACE on several RD histone transcripts in poly(A)$^+$ RNA. As seen in Figure 1D, there was an increase in the usage of a distal poly(A) site in the slow mutant compared with wild type at each of the three genes tested that was confirmed by qRT–PCR of the 3′ RACE products (Fig. 1E). Taken together, these results show that slow elongation results in increased abundance of 3′ extended poly(A)$^+$ histone transcripts.

Slow elongation results in readthrough transcription of replicative histone transcripts

We asked whether elevated expression of long polyadenylated histone transcripts in the R749H slow Pol II mutant was due to enhanced transcriptional readthrough or increased stability of these RNAs. Transcription was monitored in total nascent RNA-seq (tNetSeq) data sets derived from immunoprecipitated wild-type or R749H slow mutant Pol II (Fong et al. 2017). This analysis revealed that slow transcription caused a dramatic increase in transcriptional readthrough downstream from RD histone genes but not at non-RD histone genes that make polyadenylated mRNAs or at small nuclear RNA (snRNA) genes that make nonadenylated transcripts (Supplemental Fig.

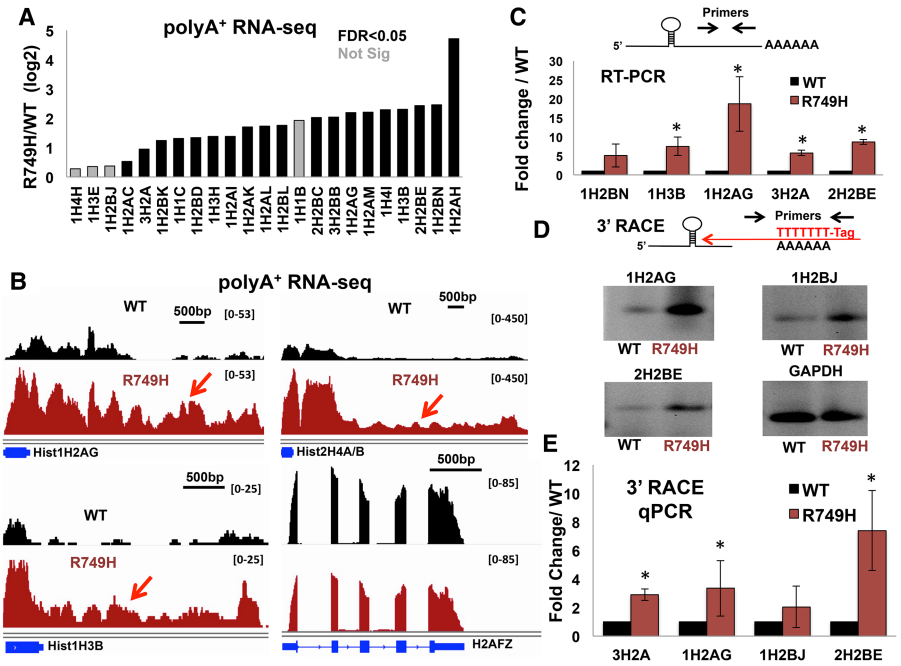

Figure 1. Slow Pol II produces 3′ extended poly(A)$^+$ histone transcripts. (*A*) Elevated poly(A)$^+$ RD histone mRNA in the R749H slow mutant. Fold change of RNA-seq reads from two replicates (FDR determined by DESeq2). (Not sig) FDR > 0.05. (*B*) Integrated Genomics Viewer (IGV) genome browser screenshots of poly(A)$^+$ RNA-seq. Genes are oriented left to right. Scale is normalized to total mapped reads for each library. Note that histone transcripts in R749H are elevated and extend beyond the normal 3′ end (red arrows). H2AFZ is a nonreplicative histone mRNA control (also see Supplemental Fig. S1A,B). Data in *A* and *B* are from Gene Expression Omnibus (GEO) GSE63375 (Fong et al. 2014). (*C*) qRT–PCR of 3′ extended poly(A)$^+$ histone mRNAs. (*D*) 3′ RACE of selected RD histone mRNAs. Note the increased use of distal poly(A) sites in the R749H slow mutant. (*E*) qRT–PCR of 3′ RACE products of selected histone genes confirms the increased use of distal poly(A) sites in R749H. (*) $P < 0.05$, Students *t*-test from three biological replicates. Error bars in *C* and *E* indicate SEM.

S1C,D). While transcription in wild-type cells terminated, on average, 350 base pairs (bp) downstream from histone genes, consistent with previous reports (Chodchoy et al. 1991; Anamika et al. 2012), in the slow mutant, transcription persisted for up to 15 kb downstream (Fig. 2A). To determine whether readthrough at histone genes was specific to the R749H mutant or a more general property of slow transcription, we examined a second slow mutant with a substitution (H1108Y) in the trigger loop domain of the large subunit. This mutant also caused readthrough of the normal termination region downstream from histone genes, as shown by tNETSeq (Fig. 2A). The failure of the R749H and H1108Y mutants to terminate transcription downstream from RD histone genes was widespread, as shown in a metaplot of 56 RD histone genes (Fig. 2B, arrow). The tNET-seq read density in the 3′ flanking region of RD histone genes in R749H was ~40% of the density at the 3′ end (Fig. 2B), indicating that in the slow mutants, almost half of histone transcripts read through the normal termination site.

We reported previously that slow Pol II mutants cause early termination downstream from most genes on the basis of anti-Pol II ChIP-seq (ChIP combined with high-throughput sequencing) (Fong et al. 2015), in contrast to histone genes, where tNET-seq revealed delayed termination. The latter result is consistent with the anti-total Pol II and anti-Ser2 phosphorylation (Ser2-P) Pol II ChIP-seq that show slightly increased Pol II occupancy at histone gene 3′ flanking regions in the R749H mutant relative to wild type (Supplemental Fig. S2A,B). In sum, these results show that slow elongation causes a defect in termination that is specific to RD histone genes and leads to extensive transcription of their 3′ flanking regions.

Slow elongation reduces SLBP recruitment to RD histone genes

We asked whether the failure to form histone mRNA 3′ ends properly could be due to failure to recruit SLBP, which is essential for 3′ cleavage of the pre-mRNA. Anti-SLBP ChIP-seq has not been reported previously, but, as expected, we found that this factor localized very specifically to RD histone genes. Specifically, SLBP localized to histone gene 3′ ends in peaks centered over the SL sequence (Fig. 3A,B). Similar results were obtained from both biologic replicates of SLBP ChIP-seq in wild-type cells (Supplemental Fig. S3A). We identified statistically significant peaks (FDR < 0.01) over the 3′ ends of 30 RD histone genes in both wild-type replicates using the MACS peak finder (Zhang et al. 2008). After filtering other SLBP ChIP-seq peaks identified by MACS for repetitive regions, no convincing SLBP ChIP-seq signal localized to any annotated genes other than RD histone genes, as reported previously for SLBP CLIP-seq (Brooks et al. 2015). The ChIP-seq

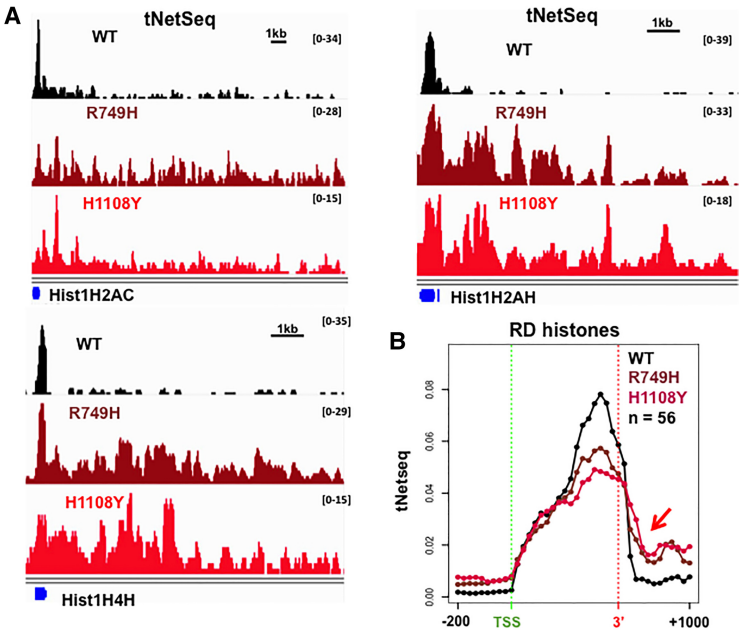

Figure 2. Slow Pol II causes readthrough transcription downstream of RD histone genes. (*A*) Screenshots of anti-Pol II tNetSeq reads in wild type and slow mutants R749H and H1108Y as in Figure 1B. Scale is normalized to total mapped reads. Note the increased readthrough transcription in the slow mutants. (*B*) Metaplot of mean histone tNetSeq signal showing increased readthrough transcription in the slow mutants (red arrow). Results in *A* and *B* are from GEO GSE97827 (Fong et al. 2017).

results are therefore consistent with the idea that SLBP recruitment is mediated by binding to the 3′ SL structure rather than through recruitment to the Pol II elongation complex prior to transcription of this element. Remarkably, examination of the ChIP results for individual histone genes and metaplots of >50 genes revealed that SLBP recruitment to RD histone genes was reduced by more than fourfold in the R749H mutant (Fig. 3A,B) in two replicate experiments (Supplemental Fig. S3A), and we were unable to detect any significant SLBP ChIP-seq peaks in genes using the MACS peak finder. This genome-wide effect on SLBP recruitment detected by ChIP-seq was confirmed by ChIP-qPCR of selected genes (Supplemental Fig. S3B).

To rule out the possibility that reduced SLBP ChIP signal was due to low expression of the protein in R749H mutant cells, we performed Western blots (Fig. 3C), which showed no detectable change in SLBP expression in untreated cells or α-amanitin-treated cells expressing the R749H mutant relative to wild type. We also observed no obvious change in total histone H3 protein levels in the slow mutant (Supplemental Fig. S3D). We conclude that SLBP is expressed at equivalent levels in wild-type and R749H Pol II mutant cells but is not stably recruited to histone genes in the slow mutant. SLBP protein levels are highly cell cycle-regulated (Whitfield et al. 2000). Therefore, the equivalent protein expression in wild-type and R749H-expressing cells (Fig. 3C) argues against a large difference in cell cycle states between wild-type and R749H cells at the time point when they were harvested. Consistent with this conclusion, expression of the cell cycle-regulated Cyclin A1 and Cyclin D1 mRNAs was unaffected in the R749H mutant, as determined by RNA-seq (Supplemental Fig. S3C). SLBP localization within cells is regulated by monoubiquitylation catalyzed by $CRL4^{WDR23}$ (Brodersen et al. 2016). We observed no transcriptional, splicing, or mRNA abundance changes for $CRL4^{WDR23}$ in R749H-expressing cells compared with wild type in our poly(A)$^+$ RNA-seq and tNET-seq data sets (data not shown). Therefore, it is unlikely that altered SLBP ubiquitylation is responsible for its failure to localize at histone genes in the slow mutant.

We also considered the possibility that SLBP recruitment was decreased in R749H cells as a result of defective recruitment of NELF, which facilitates histone mRNA 3′ end formation and termination (Narita et al. 2007). In contrast to SLBP, anti-NELF-A ChIP-seq revealed strong localization near the transcription start site (TSS) in both wild type and the R749H mutant (Fig. 3D), although we noted that NELF-A was shifted slightly upstream on histone genes in R749H compared with wild type, possibly due to the longer dwell time of slow Pol II at the 5′ end (Fong et al. 2017). These results indicate that reduced SLBP localization in the slow Pol II mutant is not accounted for by a defect in NELF recruitment.

Knockdown of CDK9, which phosphorylates Pol II CTD Ser2 residues, inhibits histone mRNA 3′ end formation (Pirngruber et al. 2009; Hsin et al. 2011). We asked whether the R749H mutation affected Ser2-P on histone genes by examining available ChIP-seq results (Fong et al. 2017). Metaplots of RD histone genes showed similar overall levels of CTD Ser2-P on histone genes in wild type and the R749H mutant, but it was shifted toward 5′ ends in R749H (Supplemental Fig. S2B) as on other protein-coding genes (Fong et al. 2017). To confirm that the Ser2-P CTD of the slow mutant was capable of recruiting canonical 3′ end processing factors, we performed ChIP-seq for CstF77 that localizes to transcribed histone genes (Glover-Cutter et al. 2008). Inspection of metaplots and individual histone genes (Fig. 3E,F) showed that transcription by slow Pol II allowed CstF77 recruitment to histone gene bodies at levels comparable with wild type. We did

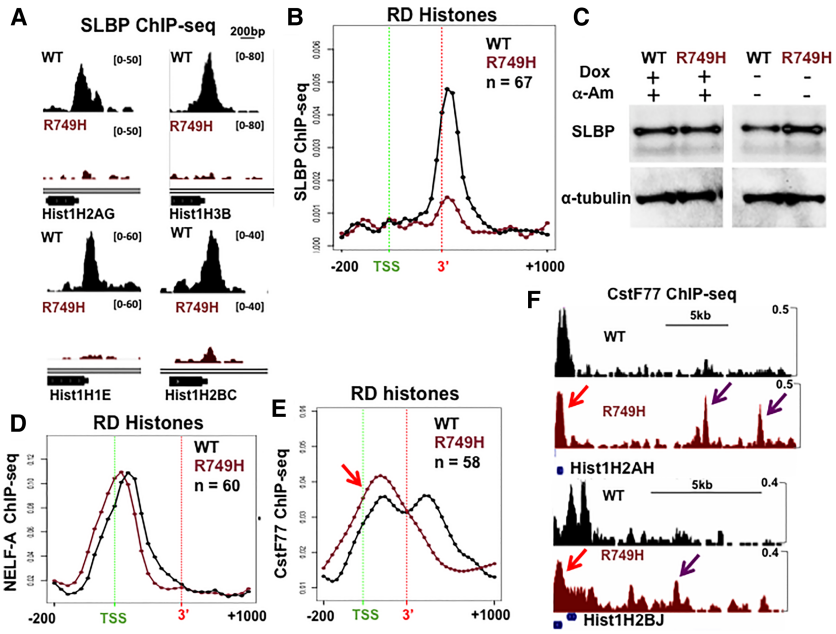

Figure 3. Slow Pol II prevents SLBP recruitment to histone genes. (*A*) IGV screenshots of SLBP ChIP-seq signal normalized to total mapped reads on histone genes in wild type and R749H. Note the loss of SLBP signal in R749H. (*B*) Metaplot of mean SLBP ChIP signals in wild type and R749H (50-bp bins). (*C*) Western blot of total protein probed with anti-SLBP and α-tubulin as a loading control. Note SLBP expression is approximately equivalent in cells expressing wild-type and R749H mutant Pol II after treatment with doxycycline (Dox) and α-amanitin (α-Am; 45 h). (*D*) Metaplots of NELF-A ChIP-seq signals on histone genes show localization in wild type and the slow R749H mutant. (*E*) Metaplots of CstF77 ChIP signals on histone genes showing a 5′ shift of occupancy in the slow mutant (red arrow). (*F*) University of California at Santa Cruz (UCSC) genome browser screenshots of CstF77 ChIP-seq on RD histone genes. Note the 5′ shift of CstF77 density in R749H (red arrows) and the increased density at downstream distal poly(A) sites (purple arrows).

note that the CstF77 ChIP signal was shifted slightly upstream in R749H compared with wild-type cells (Fig. 3E, F, red arrows), possibly due to increased dwell time and CTD Ser2-P at 5′ ends when transcription is slow (Fong et al. 2017). Interestingly, CstF77 density in the R749H mutant decreased at the 3′ ends of histone genes (Fig. 3E) and increased at distal poly(A) sites (Fig. 3F purple arrows; Supplemental Fig. S2C,D) relative to wild-type, consistent with downstream polyadenylation. In summary, these results indicate that the CTD of the R749H mutant is still highly phosphorylated on Ser2 at RD histone genes (Supplemental Fig. S2B) and facilitates recruitment of canonical 3′ end formation factors (Fig. 3E,F), arguing against a change in this modification as the cause of defective 3′ end formation.

Slow elongation disrupts histone SL folding in nascent RNA

Because reduced SLBP recruitment in the slow mutant was not readily explained by reduced expression or an indirect effect of failed NELF recruitment, we considered the possibility that the problem lay with the nascent histone RNA structure. The SL is absolutely required for SLBP association (Williams and Marzluff 1995), and we hypothesized that slow elongation could impair the cotranscriptional folding of this structure. To test this idea, we performed chemical probing with reagents that specifically modify ssRNA (selective 2′-hydroxyl acylation analyzed by primer extension and mutational profiling [SHAPE-MaP]) (Smola et al. 2015) on nascent RNA associated with wild-type and R749H mutant Pol II. As outlined in Figure 4A, nascent RNA was isolated by immunoprecipitation of Pol II (Fong et al. 2017), and the deproteinized RNA was treated with 1-methyl-7-nitroisatoic anhydride (1M7) that modifies mobile 2′ OH groups or dimethyl sulfate (DMS) that methylates unpaired A and C at N1 and N3 positions, respectively. Random primed cDNA synthesis from chemically treated RNA and untreated controls was performed under conditions that produce mutations (mismatches, insertions, and deletions) at sites of modification (Smola et al. 2015). We enriched for the 3′ ends of 30 well-expressed histone genes by PCR amplification. As a positive control, we also amplified a segment of 18S ribosomal RNA (rRNA) that is present as a contaminant in the anti-Pol II immunoprecipitations and has a known secondary structure. The reactivity of each position was determined by subtracting the percentage mutated in the untreated control from that in the 1M7- or DMS-treated sample (see the Materials and Methods).

The probing of 18S rRNA with 1M7 and DMS confirmed the known structure and showed no systematic difference in reactivity of RNA from cells expressing wild-type and R749H Pol II (Fig. 4B) or in 18S rRNA folding, as expected, because it is transcribed by Pol I. There was also good agreement between the reactivity profiles of 1M7 and DMS in the 18S transcript, as expected, since they both target single-stranded regions. Independent replicates of DMS- and 1M7-treated samples showed high reproducibility (Supplemental Fig. S4A,B). As expected, DMS preferentially modified A and C residues, while 1M7 showed no nucleotide preference (Supplemental Fig. S4C,D). The majority of both the 1M7 and DMS reactivity occurred in single-stranded regions of the previously determined 18S rRNA structure (Cannone et al. 2002), although there were some regions modified by both 1M7 and DMS that are base-paired in the mature 18S structure (Fig. 4C, asterisks). This discrepancy might be because our immunoprecipitations were prepared from nuclei that contain rRNA precursors and intermediates in ribosome assembly.

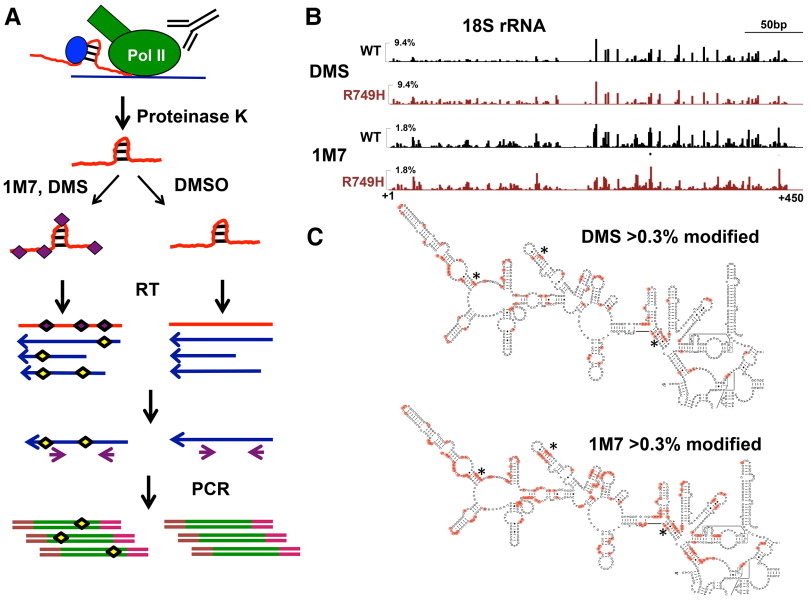

Figure 4. Chemical probing of RNA structure. (*A*) SHAPE-MaP probing of Pol II nascent transcripts. (*B*) Normalized reactivity of 18S rRNA (1–450) in anti-Pol II immunoprecipitations treated with DMS or 1M7 from wild-type and R749H-expressing cells. 18S rRNA is a contaminant in the immunoprecipitations that was used as a negative control. Note the close agreement between 1M7 and DMS treatments in wild type and the R749H mutant, as expected, since rRNA is transcribed by Pol I. (*C*) SHAPE-MaP data mapped onto the structure of human 18S rRNA (Cannone et al. 2002). Only bases with >0.3% reactivity were considered reactive and are marked in red. As DMS targets only As and Cs, only those bases are shown. Asterisks indicate regions that are base-paired in the characterized structure and reactive to both 1M7 and DMS in our immunoprecipitations of nuclear extracts.

Having established that SHAPE-MaP probing with 1M7 and DMS can reliably detect RNA structures, we interrogated the histone SL. For this analysis, we combined the reactivity results of both replicates in the 30 pooled histone transcripts at all positions in the 28-base SL consensus sequence (Fig. 5A). In cells expressing wild-type Pol II, reactivity to both DMS and 1M7 at positions within the 3′ SL sequence was greatest for bases in the loop and regions 5′ and 3′ of the stem (Fig. 5B,C, black bars), as expected for ssRNA. Conversely, little or no reactivity was observed for positions within the stem region, as expected for residues that are base-paired. The reactivity profiles for wild-type nascent transcripts are therefore in good agreement with the known structure of SL and validate the SHAPE-MaP method for probing the structure of nascent Pol II transcripts.

In contrast to transcripts made by wild-type Pol II, nascent RNA associated with the R749H slow mutant was highly reactive to 1M7 and/or DMS at positions corresponding to base pairs 2–6 of the histone SL (Fig. 5B,C, base pair 1 is at the base of the stem). Indeed, chemical reactivity at some positions within the stem was higher than in the loop region. In nascent transcripts made by the slow mutant, we also observed reduced DMS and/or 1M7 reactivity at three A residues directly upstream of the stem (highlighted in red in Fig. 5B,C) that are normally single-stranded. Residues 5 and 6 make direct contact with the SLBP RNA-binding domain, and base 4 is critical for binding (Battle and Doudna 2001; Dominski et al. 2003; Tan et al. 2013). The reduced reactivity of these important A residues suggests that they preferentially adopt an alternative, more structured RNA conformation in transcripts made by the R749H mutant compared with wild-type Pol II (Fig. 5B,C blue asterisks). Multiple alternative nascent RNA structures are likely formed among histone genes when they are transcribed by slow Pol II. However, due to the small region probed in our structure analysis, we were unable to discern additional details of these alternative structures. The changes in chemical reactivity of nascent R749H transcripts observed in an average of 30 histone genes were confirmed in several individual transcripts (Supplemental Fig. S5). In summary, bases within the conserved stem and loop

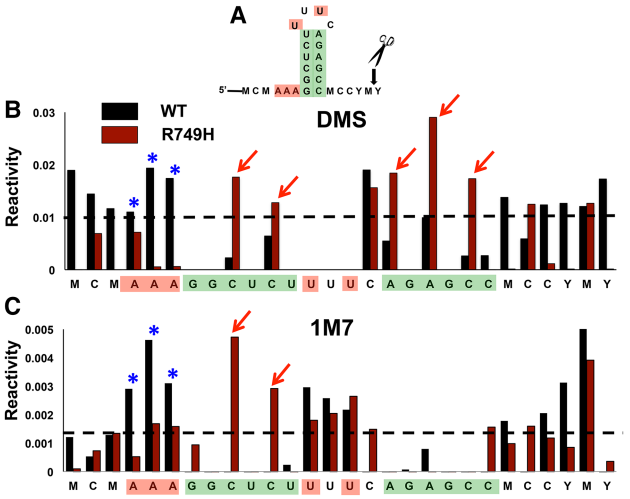

Figure 5. Slow transcription disrupts the structure of the histone 3′ SL. (*A*) Histone 3′ SL consensus sequence for 30 histone genes assayed. (M) C/A; (Y) C/U. The stem is highlighted in green, and invariant bases essential for SLBP binding are in red. (*B*,*C*) Combined reactivity (percentage modified normalized to untreated controls) of 30 well-expressed histone genes to DMS or 1M7 in nascent RNA associated with wild-type and R749H Pol II. The dashed line corresponds to the threshold of reactivity defined as one standard deviation above the mean reactivity (see the Materials and Methods). Note that reactivity is increased in the slow mutant in regions normally base-paired (red arrows) and decreased in the conserved A residues 5′ of the stem (blue asterisks).

sequences essential for 3′ processing have increased chemical reactivity in nascent RNA produced by the slow Pol II mutant. We conclude that slow transcription causes a failure in cotranscriptional folding of the SL so that it is no longer the major structure formed, and one or more alternative structures are favored where the stem region remains predominantly single-stranded and unable to bind SLBP.

UV induces slow transcription and 3′ extended poly(A)$^+$ histone transcripts

To investigate whether slow transcription induces polyadenylated histone readthrough transcripts under physiological conditions, we examined published mRNA-seq data from UV-irradiated cells. UV irradiation causes DNA damage-dependent RNA Pol II hyperphosphorylation (Munoz et al. 2017) and a marked slow down of Pol II transcription elongation that persists for at least 12 h (Munoz et al. 2009; Williamson et al. 2017). Poly(A)$^+$ transcripts of all 29 expressed histone genes were up-regulated 8 h after UV irradiation of human fibroblasts, and, for 13 transcripts, the increase was significant (FDR < 0.05), as determined by DESeq2 (Fig. 6A,B). Furthermore, the mRNA-seq reads in UV-treated cells mapped to positions that extended well beyond the normal histone gene 3′ end (Fig. 6B; Supplemental Fig. S6A). This effect of UV was specific to RD histone transcripts and was not observed for replication-independent histone genes (Supplemental Fig. S6A, bottom right panel). 3′ extended poly(A)$^+$ histone transcripts were abundant at 8 h after irradiation and declined after 24 h, consistent with recovery of normal RNA synthesis (Williamson et al. 2017). We observed similar up-regulation of 3′ extended poly(A)$^+$ histone mRNAs in an independent study of UV-irradiated human keratinocytes (Supplemental Fig. S6B,C; Shen et al. 2017). In summary, these results show that UV irradiation and slow Pol II mutants have very similar effects on expression of RD histone transcripts. Both modes of slowed elongation promote readthrough transcription and production of 3′ extended poly(A)$^+$ transcripts. We propose that altered histone mRNA 3′ end processing in UV-treated cells results from the slowing of the Pol II elongation rate that occurs under these conditions (Munoz et al. 2009; Williamson et al. 2017). These results therefore strongly suggest that physiological regulation of the elongation rate in response to an environmental stimulus can alter a cotranscriptional pre-mRNA processing event that is sensitive to nascent RNA structure.

Discussion

The rate of transcript elongation can significantly affect the outcome of cotranscriptional mRNA processing events (de la Mata et al. 2003; Fong et al. 2014; Liu et al. 2017), but how such kinetic coupling works is not well understood. One potential mechanism is through the effects of the elongation rate on folding of the nascent transcript. In this report, we show that slow transcription impairs histone mRNA 3′ end formation and termination, resulting in accumulation of 3′ extended poly(A)$^+$ transcripts. We propose that slow transcription causes this RNA processing defect by disrupting folding of the SL structure in nascent RNA that is required for binding the essential 3′ processing factor SLBP (Fig. 6C).

Localization of SLBP by ChIP-seq revealed that this RNA-binding protein binds specifically to RD histone genes, and, most importantly, binding is restricted to a discrete peak at 3′ ends of histone genes that overlaps the SL sequence (Fig. 3A,B; Supplemental Fig. S3A). This discrete localization of SLBP suggests that, unlike other 3′ end processing factors, it is not recruited to histone genes by interaction with Pol II but rather by binding to the SL structure in the nascent RNA. In support of this conclusion, SLBP was not identified by proteomic analysis as an interactor

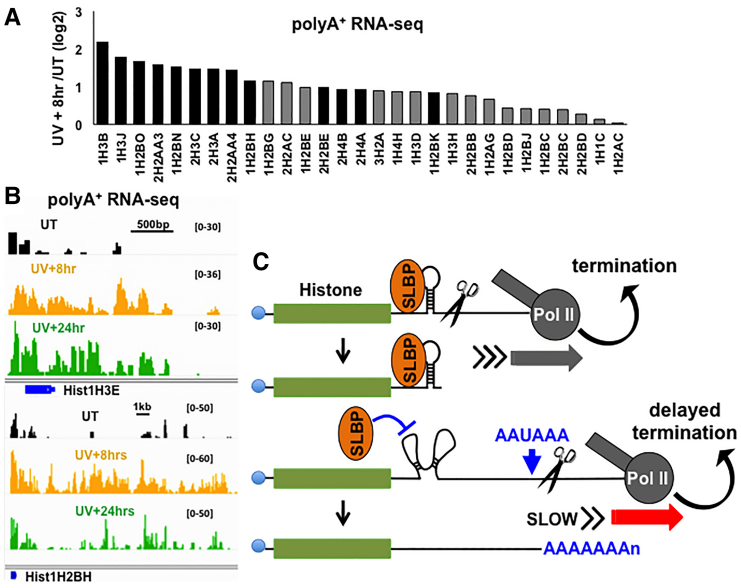

Figure 6. UV irradiation-induced slow elongation up-regulates readthrough poly(A)$^+$ histone transcripts. (*A*) UV irradiation, which slows Pol II transcription, induces production of 3′ extended poly(A)$^+$ RD histone transcripts. Fold change of poly(A)$^+$ RNA-seq reads from two replicate experiments (black bars; FDR < 0.05 determined by DESeq2). (*B*) IGV screenshots of poly(A)$^+$ RNA-seq from human fibroblasts untreated (UT) and 8 and 24 h after UV irradiation. Scale is normalized to total mapped reads. Note that after UV irradiation, poly(A)$^+$ histone transcripts are elevated and extend beyond the normal 3′ end. Results in *A* and *B* are from GEO GSE91012 (Williamson et al. 2017). (*C*) Model of elongation rate-dependent histone mRNA 3′ end formation showing a hypothetical alternative structure.

with the phosphorylated or nonphosphorylated Pol II CTD (Ebmeier et al. 2017). SLBP association with histone genes was effectively abolished when transcribed by the slow R749H mutant. This result suggests that defective histone mRNA 3′ end formation and termination in the slow mutant stem from failure to recruit SLBP. In contrast, transcription with the R749H slow polymerase did not prevent recruitment of the 3′ processing factor CstF77 (Fig. 3E) that likely associates with the elongating polymerase via the CTD (McCracken et al. 1997). SLBP is required for the optimal binding of 3′ processing factors to the histone pre-mRNA 3′ end in vitro (Skrajna et al. 2017). Together, these results suggest that slow transcription does not prevent initial recruitment of certain 3′ processing factors that probably occurs via contacts with the CTD, but, in the absence of SLBP, assembly of these factors at the SL processing site is impaired.

The localization of SLBP at the 3′ SL sequence of histone genes suggests that this secondary structure is required for SLBP binding to Pol II transcription complexes. We hypothesized that disruption of this structure might explain why SLBP fails to bind histone genes in the R749H mutant. In support of this idea, structural probing of the 3′ end of nascent RD histone transcripts showed that slow transcription increased reactivity of bases within the stem (Fig. 5), consistent with poor SL formation. We cannot completely rule out the alternative possibility that a defect in SLBP binding for other unknown reasons causes destabilization of the SL structure, but this scenario is unlikely for two reasons. First, once formed, the histone SL RNA is very stable in vitro ($\Delta G = -7.8$ kcal/mol) (Zuker 2003; Brooks et al. 2015). Second, if the 3′ end processing complex were required to stabilize the SL, then deproteinization would be predicted to unfold it, but this is not the case. The SL structure is intact in proteinase K-treated RNPs that immunoprecipitate with wild-type Pol II (Fig. 5B,C). This result therefore shows that protein association is not required for the integrity of the SL. In summary, these results favor the model that the primary defect caused by slow transcription is the failure of the nascent RNA to fold correctly into the SL structure.

While structure probing of nascent RNA made by the R749H mutant revealed that, on average, the histone mRNA 3′ SL does not fold properly, its formation may not be absolutely blocked but delayed sufficiently that a downstream poly(A) site can be processed first. One mechanism by which SL folding could be slowed or blocked is by the formation of an alternative, competing structure. This type of kinetic control of RNA folding regulates bacterial attenuation through the formation of alternative nascent RNA structures (Yanofsky 2000; Wickiser et al. 2005). Our structural probing shows that three A residues adjacent to the upstream arm of the SL that are required for SLBP binding have decreased DMS and 1M7 reactivity when transcribed by slow Pol II (bases 4–6) (Fig. 5B,C; Supplemental Fig. S5). This observation suggests that these important residues are involved in an abnormal base-pairing interaction that prevents SL formation. It is possible that inappropriate pausing by slow Pol II provides time for the nascent transcript to assume such an alternative, nonfunctional conformation, as reported previously in bacterial systems (Wickiser et al. 2005; Wong et al. 2007). It is also possible that slow transcription increases the "window of opportunity" for protein binding or RNA modification that impairs folding of the SL recognized by SLBP.

What is the physiological relevance of decreased transcription speed disrupting RD histone mRNA 3′ end formation? Several studies have shown that polyadenylated histone transcripts accumulate in response to ionizing radiation (Kari et al. 2013), serum starvation, (Pirngruber and Johnsen 2010), and terminal differentiation (Lyons et al. 2016)—conditions that are all associated with cell cycle arrest. It is possible that slow transcription elongation in cell cycle-arrested cells might help shut off normal histone mRNA 3′ end formation, thereby permitting histone mRNA expression independent of SLBP control. Consistent with this possibility, UV irradiation slows transcription elongation (Munoz et al. 2009; Williamson et al. 2017) and also causes widespread up-regulation of 3′ extended poly(A)$^+$ histone mRNAs (Fig. 6A,B; Supplemental Fig. S6). Based on the effects of the R749H Pol II mutant, we propose that this response to UV could be mediated by slow elongation that prevents folding of the histone transcript 3′ SL.

Our results reveal a previously uncharacterized phenomenon in eukaryotic cells: kinetic control of structure-dependent RNA processing through changes in nascent RNA folding. The defect in histone mRNA 3′ end formation reported here establishes a proof of principle that changes in the Pol II elongation rate can alter the way RNA folds in vivo with important consequences for the association of RNA-binding proteins and RNA processing. If slow transcription can affect the RNA folding of a small stable structure such as the histone 3′ SL, it seems reasonable that transcription speed might have additional possibly widespread effects on folding and processing of other nascent transcripts. The "rate-dependent folding and processing" principle could affect the function of RNA-binding proteins other than SLBP. This possibility is suggested by the fact that base-paired RNA sequences are globally anti-correlated with RNA-binding protein association (Taliaferro et al. 2016). "Rate-dependent folding and processing" could also apply to structure-dependent RNA processing events other than histone mRNA 3′ end formation, including splicing, cleavage/polyadenylation, A–I editing, circularization, and microRNA processing (Eperon et al. 1988; Hundley and Bass 2010; Liang and Wilusz 2014; Fernandez et al. 2017; Wu and Bartel 2017). In this context, it is relevant that 5′ and 3′ splice sites are globally associated with high and low levels of secondary structure, respectively (Wan et al. 2014), and RNA structures affect alternative splicing decisions (Eperon et al. 1988; Buratti and Baralle 2004; Buratti et al. 2004; Meyer et al. 2011; Ding et al. 2014). Furthermore, RNA structures at pre-mRNA 3′ ends correlate with increased processing because they can bring poly(A) sites into proximity with cleavage sites (Wu and Bartel 2017). Finally, our results suggest that the rate of transcription can be modulated as a mechanism to control structure-sensitive

RNA processing events in response to altered cellular conditions. This idea is suggested by the fact that slowing of Pol II elongation in response to UV is associated with inhibition of normal histone mRNA 3′ end formation and production of long poly(A)$^+$ transcripts (Fig. 6A,B; Supplemental Fig. S6). It will be of interest in the future to assess nascent RNA structure genome-wide to determine how generally rate-sensitive RNA folding modulates cotranscriptional pre-mRNA processing.

Materials and methods

Human cell lines

Flp-In-293 TREX cells (female; Invitrogen) expressing inducible α-amanitin-resistant wild-type and slow mutant Rpb1 (R749H, H1108Y) have been described (Fong et al. 2014). All experiments were performed after induction with 2.0 µg/mL doxycycline for 12–24 h and treatment with 2.5 µg/mL α-amanitin for a further 42–45 h, at which time all cell lines were viable and endogenous Pol II was inactive.

Antibodies

Rabbit anti-SLBP was a gift from Z. Dominski. Rabbit anti-NELF-A was made by immunizing with a GST fusion of human NELF-A (1–204) and affinity purification. Rat anti-tubulin was from Abcam YL1/2 (ab6160). Rabbit anti-total Pol II CTD and anti-CstF77 have been described (Schroeder et al. 2000; Glover-Cutter et al. 2008).

ChIP-seq

ChIP-seq was as described (Fong et al. 2017). For ChIP-seq data generated in this report, antibodies were used as follows (per immunoprecipitation): 5 µL of 0.3 mg/mL anti-SLBP, 7.5 µL of 0.6 mg/mL anti-CstF77 rabbit polyclonal serum, and 12.5 µL of 0.4 mg/mL anti-NELF-A with 1–3 mg of cross-linked extract. Libraries were sequenced on the Illumina Hi-Seq platform and mapped to the hg19 University of California at Santa Cruz (UCSC) human genome (February 2009) with Bowtie2 version 2.1.0 (Langmead and Salzberg 2012). A summary of ChIP-seq libraries is in Supplemental Table S3. We generated bed and wig profiles using 50-bp bins and 200-bp windows, assuming a 180-bp fragment size shifting effect. Results were viewed with the Integrated Genomics Viewer (IGV) genome browser, and metaplots were generated using R. Except where noted, metaplots show relative frequency of mean read counts per bin divided by the total number of aligned reads in all bins. The *Y*-axis of these plots represents the proportion of counts contained in each bin, and the area under each curve is equal. For histone genes, we used 20-base bins in the 5′ region from −200 to +1 relative to the TSS and 50- to 250-base bins in the 3′ region +1 to +1–5 kb as indicated on a plot relative to the 3′ end. Histone body regions were divided into 10–20 variable-length bins. Metaplots include all genes in common between the data sets for which a minimum ChIP signal was obtained. The metaplot of distal poly(A) sites contained all poly(A) sites within the human histone gene clusters showing experimental evidence of usage in poly(A)seq reads from wild type and slow mutants (chromosome 1: 149741644–149869706; chromosome 1: 228604653–228669677; chromosome 6: 25710070–25751607; chromosome 6: 26010000–26082400; chromosome 6: 26100340–26345100; chromosome 6: 27011551–27210643; chromosome 6: 27764634–27877557; and chromosome 12: 14849966–14926713) (sites were taken from N Fong and D Bentley, in prep.). All poly(A) sites falling in RD histone gene bodies or within 3 kb downstream were filtered out. The PAS density plot for histone cluster-distal poly(A) sites was generated using Homer version 4.8 (Heinz et al. 2010).

Anti-Pol II tNetSeq and targeted SHAPE-MaP

Anti-Pol II tNetSeq data were from (Fong et al. 2017) Gene Expression Omnibus (GEO) GSE97827. Targeted SHAPE-MaP (Smola et al. 2015) was performed on nascent RNA isolated by anti-Pol II immunoprecipitation (Fong et al. 2017). Immunoprecipitates were treated with 4 µg/µL proteinase K for 15 min at 37°C in 10 mM Tris-HCl (pH 8.0), 1 mM EDTA, and 0.5% SDS. 1M7 was added to 10 mM for 5 min at 37°C. DMS was added to 250 mM for 1.5 min at 37°C and stopped by addition of β-mercaptoethanol to a final concentration of 700 mM. Treated RNA was isolated using Trizol, and random primed cDNA was synthesized with SuperScript II in the presence of 6 mM $MnCl_2$, which causes mutations at modified bases (Smola et al. 2015). Sequences of the 3′ ends of histone genes (primers were placed ∼100 bp upstream of and downstream from the SL sequence) and 5′ ends of 18S rRNA were amplified by 15 cycles of PCR (see Supplemental Table S2 for primer sequences), and Illumina sequencing libraries were constructed with 15 additional PCR cycles.

SHAPE-MaP sequencing reads were uniquely mapped to the hg19 human genome or 18S rRNA using Bowtie2 version 2.1.0 (Langmead and Salzberg 2012). A summary of SHAPE-MaP libraries is in Supplemental Table S3. Mapped reads with deletions >3 bases were removed. Due to the ambiguous nature of insertions and deletions, reactivity per base was determined by counting only mismatches using pysamstats (https://github.com/alimanfoo/pysamstats) and was normalized to the total coverage per base. The reactivity of corresponding untreated samples was subtracted from the treated samples. Counts from bases with a reactivity >0.05 in any sample were removed. Reactivity of bases in the histone SL were calculated by combining the counts for each base across 30 individual histone transcripts. The normalized reactivity at which a base was considered modified (shown as dashed lines in Fig. 5B,C) was set at one standard deviation above the median normalized value averaged over wild-type and R749H samples after removing values <0 and >0.05.

qRT–PCR of 3′ extended histone transcripts

qRT–PCR was performed on three replicates of wild-type and R749H total nuclear RNA. Nuclei were isolated in 300 mM sucrose, 10 mM HEPES (pH 7.3), 85 mM KCl, 0.1 mM EDTA, 0.5% NP40, and 0.5 mM DTT. Intact nuclei were washed twice in 10 mM TE, and RNA was isolated using Trizol. Oligo-dT primed cDNA was synthesized with SuperScript IV (Invitrogen) and PCR-amplified using primers (Supplemental Table S2) within 5 kb downstream from histone genes (Fig. 1C). qPCR targets were selected based on evidence of increased readthrough transcription in mRNA-seq reads and the ability to design unique primers against potential targets. Signals were normalized to GAPDH, whose abundance is unaffected in the R749H mutant. The fold change between wild type and R749H was calculated using the $\Delta/\Delta C_t$ method.

3′ RACE and 3′ RACE qRT–PCR

Total nuclear RNA was used to generate cDNA using SuperScript IV (Invitrogen) with the dT18-XbaKpnBam primer (Supplemental Table S2). 3′ RACE (Fig. 1D) was carried out using two rounds of

PCR with nested forward primers and the XbaKpnBam reverse primer (Supplemental Table S2; Berg et al. 2012). qPCR of 3′ RACE (Fig. 1E) was performed using 1 µL of the first PCR reaction (20 cycles) amplified with a nested forward primer and the XbaKpnBam reverse primer. The fold change in signal was calculated using $\Delta/\Delta C_t$ after normalizing to GAPDH. 3′ RACE targets were selected based on evidence of increased usage of a distal poly (A) site in poly(A)seq reads from R749H compared with wild type (N Fong and D Bentley, in prep.) and the ability to design unique primers. Sequences surrounding the targeted poly(A) site are as follows, with the PAS site underlined and the approximate site of cleavage in bold: Hist2H2BE (TTAATAAAGTTACCAATT AA**TTT**AAAGGCTTTGCTGGAT), Hist1H2AG (CTAAATTC ATAATAAAGTGAAATGT**TC**AAGTTCAGTCAAG), Hist1H2BJ (TAATAGCAAATAAATTAACTTTTATG**ACAG**GGAATTGTT G), and Hist3H2A (TCTGATATTAAAAGTATTTA**TGAT**CTC TAAGTAGTTTGC).

Immunoblotting

Immunoblots were probed with rabbit anti-SLBP (1:1000; kindly provided by Z. Dominski), rat anti-tubulin, and anti-histone H3. HRP-conjugated goat anti-rabbit antibody (DAKO) was used, and signals were developed with ECL Plus (Roche).

Accession numbers

ChIP-seq and RNA-seq data sets were deposited at GEO under accession number GSE109652.

Acknowledgments

We thank K. Weeks and Z Dominski (University of North Carolina) for 1M7 and anti-SLBP antibody, and O. Rissland, M. Taliaferro, and T. Blumenthal for comments on the manuscript. We thank K. Diener, B. Gao, and the University of Colorado at Denver Sequencing Facility for sequencing. This work was supported by National Institutes of Health grant R35GM118051 to D.L.B., and American Cancer Society fellowship PF-15-188-01-RMC to T.S.

References

Anamika K, Gyenis À, Poidevin L, Poch O, Tora L. 2012. RNA polymerase II pausing downstream of core histone genes is different from genes producing polyadenylated transcripts. *PLoS ONE* **7:** e38769.

Battle DJ, Doudna JA. 2001. The stem–loop binding protein forms a highly stable and specific complex with the 3′ stem–loop of histone mRNAs. *RNA* **7:** 123–132.

Berg MG, Singh LN, Younis I, Kaida D, Zhang Z, Wan L, Dreyfuss G. 2012. U1 snRNP determines mRNA length and regulates isoform expression. *Cell* **150:** 53–64.

Birchmeier C, Grosschedl R, Birnstiel ML. 1982. Generation of authentic 3′ termini of an H2A mRNA in vivo is dependent on a short inverted DNA repeat and on spacer sequences. *Cell* **28:** 739–745.

Brodersen MML, Lampert F, Barnes CA, Soste M, Piwko W, Peter M. 2016. CRL4WDR23-mediated SLBP ubiquitylation ensures histone supply during DNA replication. *Mol Cell* **62:** 627–635.

Brooks L, Lyons SM, Mahoney JM, Welch JD, Liu Z, Marzluff WF, Whitfield ML. 2015. A multiprotein occupancy map of the mRNP on the 3′ end of histone mRNAs. *RNA* **21:** 1943–1965.

Buratti E, Baralle FE. 2004. Influence of RNA secondary structure on the pre-mRNA splicing process. *Mol Cell Biol* **24:** 10505–10514.

Buratti E, Muro AF, Giombi M, Gherbassi D, Iaconcig A, Baralle FE. 2004. RNA folding affects the recruitment of SR proteins by mouse and human polypurinic enhancer elements in the fibronectin EDA exon. *Mol Cell Biol* **24:** 1387–1400.

Cannone JJ, Subramanian S, Schnare MN, Collett JR, D'Souza LM, Du Y, Feng B, Lin N, Madabusi LV, Muller KM, et al. 2002. The comparative RNA Web (CRW) site: an online database of comparative sequence and structure information for ribosomal, intron, and other RNAs. *BMC Bioinformatics* **3:** 2.

Chao MY, Kan MC, Lin-Chao S. 1995. RNAII transcribed by IPTG-induced T7 RNA polymerase is non-functional as a replication primer for ColE1-type plasmids in *Escherichia coli*. *Nucleic Acids Res* **23:** 1691–1695.

Chodchoy N, Pandey NB, Marzluff WF. 1991. An intact histone 3′-processing site is required for transcription termination in a mouse histone H2a gene. *Mol Cell Biol* **11:** 497–509.

Danko CG, Hah N, Luo X, Martins AL, Core L, Lis JT, Siepel A, Kraus WL. 2013. Signaling pathways differentially affect RNA polymerase II initiation, pausing, and elongation rate in cells. *Mol Cell* **50:** 212–222.

de la Mata M, Alonso CR, Kadener S, Fededa JP, Blaustein M, Pelisch F, Cramer P, Bentley D, Kornblihtt AR. 2003. A slow RNA polymerase II affects alternative splicing in vivo. *Mol Cell* **12:** 525–532.

Ding Y, Tang Y, Kwok CK, Zhang Y, Bevilacqua PC, Assmann SM. 2014. In vivo genome-wide profiling of RNA secondary structure reveals novel regulatory features. *Nature* **505:** 696–700.

Dominski Z, Zheng LX, Sanchez R, Marzluff WF. 1999. Stem–loop binding protein facilitates 3′-end formation by stabilizing U7 snRNP binding to histone pre-mRNA. *Mol Cell Biol* **19:** 3561–3570.

Dominski Z, Yang X-C, Kaygun H, Dadlez M, Marzluff WF. 2003. A 3′ exonuclease that specifically interacts with the 3′ end of histone mRNA. *Mol Cell* **12:** 295–305.

Dominski Z, Yang XC, Marzluff WF. 2005. The polyadenylation factor CPSF-73 is involved in histone-pre-mRNA processing. *Cell* **123:** 37–48.

Ebmeier CC, Erickson B, Allen BL, Allen MA, Kim H, Fong N, Jacobsen JR, Liang K, Shilatifard A, Dowell RD, et al. 2017. Human TFIIH kinase CDK7 regulates transcription-associated chromatin modifications. *Cell Rep* **20:** 1173–1186.

Eggington JM, Greene T, Bass BL. 2011. Predicting sites of ADAR editing in double-stranded RNA. *Nat Commun* **2:** 319.

Eperon LP, Graham IR, Griffiths AD, Eperon IC. 1988. Effects of RNA secondary structure on alternative splicing of pre-mRNA: is folding limited to a region behind the transcribing RNA polymerase? *Cell* **54:** 393–401.

Fernandez N, Cordiner RA, Young RS, Hug N, Macias S, Caceres JF. 2017. Genetic variation and RNA structure regulate microRNA biogenesis. *Nat Commun* **8:** 15114.

Fong N, Kim H, Zhou Y, Ji X, Qiu J, Saldi T, Diener K, Jones K, Fu XD, Bentley DL. 2014. Pre-mRNA splicing is facilitated by an optimal RNA polymerase II elongation rate. *Genes Dev* **28:** 2663–2676.

Fong N, Brannan K, Erickson B, Kim H, Cortazar MA, Sheridan RM, Nguyen T, Karp S, Bentley DL. 2015. Effects of transcription elongation rate and Xrn2 exonuclease activity on RNA polymerase II termination suggest widespread kinetic competition. *Mol Cell* **60:** 256–267.

Fong N, Saldi T, Sheridan RM, Cortazar MA, Bentley DL. 2017. RNA Pol II dynamics modulate co-transcriptional chromatin

modification, CTD phosphorylation, and transcriptional direction. *Mol Cell* **66:** 546–557.

Fuchs G, Voichek Y, Benjamin S, Gilad S, Amit I, Oren M. 2014. 4sUDRB-seq: measuring genomewide transcriptional elongation rates and initiation frequencies within cells. *Genome Biol* **15:** R69.

Glover-Cutter K, Kim S, Espinosa J, Bentley DL. 2008. RNA polymerase II pauses and associates with pre-mRNA processing factors at both ends of genes. *Nat Struct Mol Biol* **15:** 71–78.

Heinz S, Benner C, Spann N, Bertolino E, Lin YC, Laslo P, Cheng JX, Murre C, Singh H, Glass CK. 2010. Simple combinations of lineage-determining transcription factors prime cis-regulatory elements required for macrophage and B cell identities. *Mol Cell* **38:** 576–589.

Hsin J-P, Sheth A, Manley JL. 2011. RNAP II CTD phosphorylated on threonine-4 is required for histone mRNA 3′ end processing. *Science* **334:** 683–686.

Hundley HA, Bass BL. 2010. ADAR editing in double-stranded UTRs and other noncoding RNA sequences. *Trends Biochem Sci* **35:** 377–383.

Ip JY, Schmidt D, Pan Q, Ramani AK, Fraser AG, Odom DT, Blencowe BJ. 2011. Global impact of RNA polymerase II elongation inhibition on alternative splicing regulation. *Genome Res* **21:** 390–401.

Kari V, Karpiuk O, Tieg B, Kriegs M, Dikomey E, Krebber H, Begus-Nahrmann Y, Johnsen SA. 2013. A subset of histone H2B genes produces polyadenylated mRNAs under a variety of cellular conditions. *PLoS One* **8:** e63745.

Koduvayur SP, Woodson SA. 2004. Intracellular folding of the *Tetrahymena* group I intron depends on exon sequence and promoter choice. *RNA* **10:** 1526–1532.

Kolev NG, Steitz JA. 2005. Symplekin and multiple other polyadenylation factors participate in 3′-end maturation of histone mRNAs. *Genes Dev* **19:** 2583–2592.

Lai D, Proctor JR, Meyer IM. 2013. On the importance of cotranscriptional RNA structure formation. *RNA* **19:** 1461–1473.

Langmead B, Salzberg SL. 2012. Fast gapped-read alignment with Bowtie 2. *Nat Methods* **9:** 357–359.

Lanzotti DJ, Kaygun H, Yang X, Duronio RJ, Marzluff WF. 2002. Developmental control of histone mRNA and dSLBP synthesis during *Drosophila* embryogenesis and the role of dSLBP in histone mRNA 3′end processing in vivo. *Mol Cell Biol* **22:** 2267–2282.

Lewicki BT, Margus T, Remme J, Nierhaus KH. 1993. Coupling of rRNA transcription and ribosomal assembly in vivo. Formation of active ribosomal subunits in *Escherichia coli* requires transcription of rRNA genes by host RNA polymerase which cannot be replaced by bacteriophage T7 RNA polymerase. *J Mol Biol* **231:** 581–593.

Liang D, Wilusz JE. 2014. Short intronic repeat sequences facilitate circular RNA production. *Genes Dev* **28:** 2233–2247.

Liu X, Freitas J, Zheng D, Hoque M, Oliveira MS, Martins T, Henriques T, Tian B, Moreira A. 2017. Transcription elongation rate has a tissue-specific impact on alternative cleavage and polyadenylation in *Drosophila melanogaster*. *RNA* **23:** 1807–1816.

Lyons SM, Cunningham CH, Welch JD, Groh B, Guo AY, Wei B, Whitfield ML, Xiong Y, Marzluff WF. 2016. A subset of replication-dependent histone mRNAs are expressed as polyadenylated RNAs in terminally differentiated tissues. *Nucleic Acids Res* **44:** 9190–9205.

McCracken S, Fong N, Yankulov K, Ballantyne S, Pan G, Greenblatt J, Patterson SD, Wickens M, Bentley DL. 1997. The C-terminal domain of RNA polymerase II couples mRNA processing to transcription. *Nature* **385:** 357–361.

Meyer M, Plass M, Perez-Valle J, Eyras E, Vilardell J. 2011. Deciphering 3′ss selection in the yeast genome reveals an RNA thermosensor that mediates alternative splicing. *Mol Cell* **43:** 1033–1039.

Mowry KL, Steitz JA. 1987. Identification of the human U7 snRNP as one of several factors involved in the 3′ end maturation of histone premessenger RNA's. *Science* **238:** 1682–1687.

Munoz MJ, Perez Santangelo MS, Paronetto MP, de la Mata M, Pelisch F, Boireau S, Glover-Cutter K, Ben-Dov C, Blaustein M, Lozano JJ, et al. 2009. DNA damage regulates alternative splicing through inhibition of RNA polymerase II elongation. *Cell* **137:** 708–720.

Munoz MJ, Nieto Moreno N, Giono LE, Cambindo Botto AE, Dujardin G, Bastianello G, Lavore S, Torres-Mendez A, Menck CFM, Blencowe BJ, et al. 2017. Major roles for pyrimidine dimers, nucleotide excision repair, and ATR in the alternative splicing response to UV irradiation. *Cell Rep* **18:** 2868–2879.

Narita T, Yung TM, Yamamoto J, Tsuboi Y, Tanabe H, Tanaka K, Yamaguchi Y, Handa H. 2007. NELF interacts with CBC and participates in 3′ end processing of replication-dependent histone mRNAs. *Mol Cell* **26:** 349–365.

Pan T, Sosnick T. 2006. RNA folding during transcription. *Annu Rev Biophys Biomol Struct* **35:** 161–175.

Pan T, Artsimovitch I, Fang XW, Landick R, Sosnick TR. 1999. Folding of a large ribozyme during transcription and the effect of the elongation factor NusA. *Proc Natl Acad Sci* **96:** 9545–9550.

Pinto PA, Henriques T, Freitas MO, Martins T, Domingues RG, Wyrzykowska PS, Coelho PA, Carmo AM, Sunkel CE, Proudfoot NJ, et al. 2011. RNA polymerase II kinetics in polo polyadenylation signal selection. *EMBO J* **30:** 2431–2444.

Pirngruber J, Johnsen SA. 2010. Induced G1 cell-cycle arrest controls replication-dependent histone mRNA 3′ end processing through p21, NPAT and CDK9. *Oncogene* **29:** 2853–2863.

Pirngruber J, Shchebet A, Schreiber L, Shema E, Minsky N, Chapman RD, Eick D, Aylon Y, Oren M, Johnsen SA. 2009. CDK9 directs H2B monoubiquitination and controls replication-dependent histone mRNA 3′-end processing. *EMBO Rep* **10:** 894–900.

Repsilber D, Wiese S, Rachen M, Schroder AW, Riesner D, Steger G. 1999. Formation of metastable RNA structures by sequential folding during transcription: time-resolved structural analysis of potato spindle tuber viroid (-)-stranded RNA by temperature-gradient gel electrophoresis. *RNA* **5:** 574–584.

Schaufele F, Gilmartin GM, Bannwarth W, Birnstiel ML. 1986. Compensatory mutations suggest that base-pairing with a small nuclear RNA is required to form the 3′ end of H3 messenger RNA. *Nature* **323:** 777–781.

Schroeder SC, Schwer B, Shuman S, Bentley D. 2000. Dynamic association of capping enzymes with transcribing RNA polymerase II. *Genes Dev* **14:** 2435–2440.

Shen Y, Stanislauskas M, Li G, Zheng D, Liu L. 2017. Epigenetic and genetic dissections of UV-induced global gene dysregulation in skin cells through multi-omics analyses. *Sci Rep* **7:** 42646.

Skrajna A, Yang X-C, Bucholc K, Zhang J, Hall TMT, Dadlez M, Marzluff WF, Dominski Z. 2017. U7 snRNP is recruited to histone pre-mRNA in a FLASH-dependent manner by two separate regions of the stem–loop binding protein. *RNA* **23:** 938–951.

Smola MJ, Rice GM, Busan S, Siegfried NA, Weeks KM. 2015. Selective 2′-hydroxyl acylation analyzed by primer extension and mutational profiling (SHAPE-MaP) for direct, versatile and accurate RNA structure analysis. *Nat Protoc* **10:** 1643–1669.

Sullivan KD, Steiniger M, Marzluff WF. 2009. A core complex of CPSF73, CPSF100, and Symplekin may form two different cleavage factors for processing of poly(A) and histone mRNAs. *Mol Cell* **34:** 322–332.

Taliaferro JM, Lambert NJ, Sudmant PH, Dominguez D, Merkin JJ, Alexis MS, Bazile CA, Burge CB. 2016. RNA sequence context effects measured in vitro predict in vivo protein binding and regulation. *Mol Cell* **64:** 294–306.

Tan D, Marzluff WF, Dominski Z, Tong L. 2013. Structure of histone mRNA stem–loop, human stem–loop binding protein, and 3′hExo ternary complex. *Science* **339:** 318–321.

Wan Y, Qu K, Zhang QC, Flynn RA, Manor O, Ouyang Z, Zhang J, Spitale RC, Snyder MP, Segal E, et al. 2014. Landscape and variation of RNA secondary structure across the human transcriptome. *Nature* **505:** 706–709.

Wang ZF, Whitfield ML, Ingledue TC, Dominski Z, Marzluff WF. 1996. The protein that binds the 3′-end of histone messenger-RNA—a novel RNA-binding protein required for histone pre-Messenger-RNA processing. *Genes Dev* **10:** 3028–3040.

Whitfield ML, Zheng LX, Baldwin A, Ohta T, Hurt MM, Marzluff WF. 2000. Stem–loop binding protein, the protein that binds the 3′ end of histone mRNA, is cell cycle regulated by both translational and posttranslational mechanisms. *Mol Cell Biol* **20:** 4188–4198.

Wickiser JK, Winkler WC, Breaker RR, Crothers DM. 2005. The speed of RNA transcription and metabolite binding kinetics operate an FMN riboswitch. *Mol Cell* **18:** 49–60.

Williams AS, Marzluff WF. 1995. The sequence of the stem and flanking sequences at the 3′ end of histone mRNA are critical determinants for the binding of the stem–loop binding protein. *Nucleic Acids Res* **23:** 654–662.

Williams AS, Ingledue TC III, Kay BK, Marzluff WF. 1994. Changes in the stem–loop at the 3′ terminus of histone mRNA affects its nucleocytoplasmic transport and cytoplasmic regulation. *Nucleic Acids Res* **22:** 4660–4666.

Williamson L, Saponaro M, Boeing S, East P, Mitter R, Kantidakis T, Kelly GP, Lobley A, Walker J, Spencer-Dene B, et al. 2017. UV irradiation induces a non-coding RNA that functionally opposes the protein encoded by the same gene. *Cell* **168:** 843–855.

Wong EM, Polisky B. 1985. Alternative conformations of the ColE1 replication primer modulate its interaction with RNA I. *Cell* **42:** 959–966.

Wong TN, Sosnick TR, Pan T. 2007. Folding of noncoding RNAs during transcription facilitated by pausing-induced nonnative structures. *Proc Natl Acad Sci* **104:** 17995–18000.

Wu X, Bartel DP. 2017. Widespread influence of 3′-end structures on mammalian mRNA processing and stability. *Cell* **169:** 905–917.

Yang X-C, Sabath I, Debski J, Kaus-Drobek M, Dadlez M, Marzluff WF, Dominski Z. 2012. A complex containing the CPSF73 endonuclease and other polyadenylation factors associates with U7 snRNP and is recruited to histone pre-mRNA for 3′-end processing. *Mol Cell Biol* **33:** 28–37.

Yanofsky C. 2000. Transcription attenuation: once viewed as a novel regulatory strategy. *J Bacteriol* **182:** 1–8.

Zhang Y, Liu T, Meyer CA, Eeckhoute J, Johnson DS, Bernstein BE, Nusbaum C, Myers RM, Brown M, Li W, et al. 2008. Model-based analysis of ChIP-seq (MACS). *Genome Biol* **9:** R137.

Zuker M. 2003. Mfold Web server for nucleic acid folding and hybridization prediction. *Nucleic Acids Res* **31:** 3406–3415.